Techniques to safeguard the Underground Tunnels against Surface Blast load

[a]K. Senthil, [a]M. Sethi, [b]L. Pelecanos

[a] Department of Civil Engineering, Dr. BR Ambedkar NIT Jalandhar, Punjab 144011, India

[b] Department of Architecture and Civil Engineering, University of Bath, Bath, UK.

Abstract

Due to the growth of underground tunnels, the safety of structures under blast loading is a major threat. Therefore, this paper focused on various techniques such as tunnel burial depth, tunnel shape, tunnel lining materials and varying the location of the blast source to safeguard underground tunnels against blast load using numerical analysis. The behavior of concrete, reinforcement steel and the soil were incorporated by using the different constitutive model available in ABAQUS v. 2020. The predicted results were compared with the experimental results available in literature and found in close agreement. It is concluded that the layering of soil filling and depth of the burial of the tunnel found to be most important in case of external blast, whereas the stress bearing capacity of the concrete found to be important in case of internal blast. It is also concluded that the circular shape tunnel is one of the best performing tunnels.

Keywords: Tunnels, Blast Load, Burial depth, Lining Materials, Tunnel Shape, Blast Location

1. Introduction

The use of underground tunnels is getting common for various purposes to satisfy the demands of increasing population. The underground tunnels are being used for the transportation of various goods and commodities as well as for the movement of people from one place to another. With increasing use and popularity, the underground tunnels are always prone to the attacks by the enemies or natural calamities. Hence it is very important to predict and evaluate the damage being caused to the underground tunnels, as an effect of blast loading. **Zhao et al. (2010)** proposed a simple method for designing of concrete lining in tunnels subjected to explosive detonation on ground surface or explosion of a projectile penetrating into the ground located adjacent to the tunnel. The proposed method comprises of shotcrete/rockbolt support system, based on the single degree of freedom approach, which prevents the occurrence of spalling due to blast loads. The method follows a step by step procedure and avoid the usage of complex numerical calculations. **Yang et al. (2010)** studied

the dynamic behavior of circular metro tunnel against surface detonation. It was observed that the upper part is considered the most vulnerable in comparison to other parts of the tunnel against the detonation. Also, it was concluded that, if a surface explosion contains less than 500 Kg of TNT, then a lining thickness equal to 350 mm is considered the safe for depths more than 7m.

Xia et al. (2013) predicted the amount of damage to rocks and the reinforced shotcrete lining structure by the influence of an adjacent excavation blasting, in Damaoshan highway tunnel. It was observed that for the peak particle velocity less than 0.3 m/s, no failure occurred in the existing tunnel and at the rocks-lining interface. **Mobaraki and Vaghefi (2015)** investigated the effect of surface explosion on Kobe box shaped tunnel and compared the results with that of semi ellipse, horse shoe shaped and circular tunnel. It was observed that circular and horseshoe shaped tunnels show less resistance to demolition than box shaped tunnel, however the semi ellipse tunnel shows more resistance than box shaped tunnel. **Yu et al. (2015)** investigated on square and circular shape's tunnel responses against internal explosion. It was observed that the maximum effective plastic strain response at the critical points (i.e. at the structural corner of tunnel and center of top plate) of square tunnel are significantly lower as compared to the circular tunnel. **Tiwari et al. (2016)** studied the damage caused to RC lining as well as the rocks surrounding the tunnel subjected to internal blast loading. It was observed that the rocks surrounding the tunnel experience higher stress due to damage in RC lining. Higher attenuation of shock wave is shown by the rocks having high weathering conditions and low modulus. **Gao et al. (2016)** observed a decrease in dynamic responses shown by cylindrical tunnels in an oscillating manner, when the time elapses. However, these responses attenuate exponentially by increasing the distance between the explosion source and the tunnel.

Khan et al. (2016) studied the tunnels made up of cast iron lining and subjected to internal blast loading. The blast response of tunnels was found affected significantly by tunnel lining thickness, peak blast pressure and soil and rock elastic moduli. The corresponding results were found less affected by soil and rock dilation angle. It was recommended that in order to create a blast resistant tunnel design, an increase in the lining thickness shall be viable option. **Dang et al. (2018)** studied the damage caused to the concrete lining of an existing tunnel, due to the blasting activities used for the construction of a new adjacent tunnel. It was observed that the tunnel side facing the blast source undergoes greater damage as compared to the face of tunnel away from the blast source. It was concluded that, more is the distance between the blast source and the existing tunnel face, more is the safety of the concrete lining in the existing

tunnel. **Hu et al. (2018)** proposed a model to study the vibration response shown by concrete segmental tunnel lining against internal blast loading acting axisymmetrically. During the expansion deformation process, stiffness of the joint bolt plays an essential role. For the case of contraction phase, all the compression effect is taken by the concrete segments. **Majumder and Bhattacharya (2019)** studied the performance of intermittent geofoam infilled trench as a passive vibration screening method for a reinforced concrete lining tunnel subjected to internal blast loading. It was concluded that the trench installed with passive vibration screening technique shall help in the reduction of blast waves causing ground vibrations.

Ambrosini and Luccioni(2019) studied about the propagation of shock waves in the soil and the main phenomenon taken under consideration were formation of shock waves, propagation of elastic plastic wave in the soil and interaction between soil and structures. It was observed that the properties of soil play a major role to determine the propagation of shock waves in the soil. However, the soil properties have an insignificant effect on the diameter of the crater. **Bettelini (2019)** proposed a holistic approach to ensure the safety in underground tunnel networks against risks generated by natural phenomenon (eg- gas radiation, temperature rise, lack of oxygen) or human activities (eg- smoke, fire, terrorist explosions or structure failure). It was observed that the safety proposals comprised providing safety barriers against hazards and multiple protection layers to reduce the harm generated by hazards. **Vinod and Khabbaz (2019)** compared the surface settlements and moments generated while boring of circular and rectangular twin tunnels in weak ground. It was observed that, for weak grounds and shallow depths, rectangular tunnels show lesser settlements in comparison to circular tunnels. However, higher bending moments are produced in rectangular tunnels compared to circular tunnels. **Prasanna and Boominathan (2020)** observed lesser damage in cast iron tunnels as compared to RCC tunnels subjected to internal blast loading. The reason may be due to the higher stiffness and density is possessed by cast iron tunnels than RCC tunnels. **Jagriti Mandal et al. (2020)** found that 10% decrease in peak displacement in case of circular cross section tunnel and it may be due to less reflected pressure waves were generated on circular surface compared to box shaped and horseshoe shape tunnel. **Liu et al. (2020)** considered the effect of blast load used for the construction of a new tunnel adjacent to an existing circular highway tunnel named Huanglongshan. The peak particle velocity of the lining structure present in the existing tunnel was studied. It was observed that the peak particle velocity value was higher at the face located infront of the blast source as compared to the face placed behind the blast source. **Goel et al. (2020)** carried out finite element analysis for comparison of the damage caused to the tunnel and surrounding soil considering three different tunnel cross

sections i.e. arched, circular and rectangular using 100 Kg TNT explosive for saturated and unsaturated soil conditions. It was observed that arched as well as rectangular lining experienced 29.56% and 50.31% more displacement compared to the circular lining on the top node of the tunnel lining without any change in other parameters. **Ata et al. (2021)** studied the effect of blast loading by considering the mass of TNT as 100, 200, 300 and 400 Kg. An increase of 64% of kinetic energy was observed when the charge weight was increased from 100 to 400 Kg. **Mandal et al. (2021)** observed an increase in the displacement at tunnel roof center by 94 and 324% by increasing the charge weight from 250 to 500 Kg and 1000 Kg respectively.

Zhang et al. (2021) proposed a study based on andesitic porphyrite failure rule adopted by the technique of open cut blasting in reservoir tunnel. It was observed by test results as well as the numerical analysis that, blasting excavation through andesitic porphyrite proved to be suitable for just 1-2 areas.

Based on the detailed literature review, it was observed that the investigations on the evaluation of mitigation strategies on tunnels against surface blast loading are limited. Also, the studies revealed that the influence of tunnel burial depth, influence of tunnel shapes and influence of different tunnel lining materials subjected to external surface blast loading are found to be limited. Therefore, this paper is focused on the prediction of mitigation strategies of underground tunnels against surface blast loading using finite element technique, ABAQUS Explicit software v. 2020. The concrete, reinforcement steel and the soil were modelled and the constitutive behavior was incorporated using the model such as Concrete Damage Plasticity Model, Johnson Cook Model and Drucker Prager model respectively, see **Section 2** and **Section 3.** The results in terms of acceleration thus predicted were compared with the experimental results available in the literature, see **Section 4**. Further, the simulations were conducted by varying tunnel burial depth, tunnel shape, tunnel lining materials and varying the location of the blast source in order to estimate the mitigation strategies of the underground tunnels, see **Section 5.**

2. Constitutive Modelling

The constitutive model and the material behaviour such as concrete, metals and soil are discussed in this Section. The inelastic behaviour of concrete was modelled by using Concrete Damage Plasticity model, available in ABAQUS/Explicit. The Johnson-Cook model was used to incorporate the elastic and plastic behaviour of steel reinforcement bars as well as lining

materials of aluminium alloy. The Drucker Prager model was used to model the soil elements are discussed here.

2.1 Johnson-Cook model for Aluminium and Steel Reinforcement

Johnson-Cook elasto- viscoplastic material model, available in ABAQUS/Explicit v. 2020 is used to predict the flow and fracture behaviour of aluminium alloy and steel reinforcement bars. The model is based on the criteria of associated flow rule and von Mises yield criterion. The effects of thermo-elasticity, plastic flow, yielding, isotropic strain hardening, strain rate hardening, softening due to adiabatic heating and damage are included in this model. Various constants are used to define the Johnson Cook model, which comprises of initial yield of the material, strain hardening coefficient, strain hardening exponent, strain rate sensitivity and thermal softening parameter, denoted by A, B, C and m respectively. The Johnson-cook material parameters for aluminium as well as steel reinforcement are given in **Table 1.** This model can also be used along with some damage and failure models, due to the provision of which certain damage initiation criteria can be specified. Further, a smooth degradation of the material can be supported by the progressive damage models, hence making the materials suited for dynamic and quasi-static situations. The elements possessing displacement degree of freedom as available in ABAQUS software can support the use of Johnson-Cook model.

2.2 Concrete Damaged Plasticity Model for Concrete

The inelastic behaviour of concrete is modelled by using concrete damaged plasticity model, which incorporates both tensile and compressive behaviour of concrete. This model can appropriately define the inelastic behaviour of concrete, based on the concept of elastic damage in combination with isotropic expansion and compression flexibility. This model can be used to define the behaviour of both reinforced concrete as well as plain concrete. This model can be used to define the concrete behaviour, also with that of the presence of rebars to define reinforced concrete. This model may help to define the behaviour of concrete, subjected to monotonic cyclic or dynamic loading conditions under low confining pressures. The model can also be defined, being sensitive to the strain rate. The two main failure mechanisms, including tensile cracking and compressive crushing of the concrete material are assumed by this model. Two hardening variables namely ε_c^{pl} and ε_t^{pl} which are compressive and tensile equivalent plastic strains, respectively control the evolution of the yield surface and are linked to failure mechanisms under tension and compression loading. The damage variable values can vary

from zero to one, where zero represents the undamaged material and one represents total loss of strength. This model works on the principle of isotropic and linear damage of concrete, which is subjected to arbitrary loading conditions. The stress strain relations under uniaxial compression and tension loading are given by the following equations where E_o is the initial (undamaged) elastic stiffness of the material: $\sigma_t = (1-d_t)E_o(\varepsilon_t-\varepsilon_t^{pl})$ and $\sigma_c = (1-d_c)E_o(\varepsilon_c-\varepsilon_c^{pl})$, where d_t and d_c are tension damage variable and compression damage variable respectively. The concrete damaged plasticity model parameters for concrete are given in **Table 2-6.**

2.3 Drucker-Prager model for soil

Drucker-Prager model is the simplification of Mohr-Coulomb model, where the hexagonal shaped failure cone was replaced by a simple cone. The circular yield is possessed by the Drucker-Prager model, which is equidistant from the center to the yield surface. The yield area in this model consists of two main areas i.e. the fracture area providing the flow cut and the cover, crossing the equivalent pressure. This model is based on Drucker Prager yield criteria, which is used to detect if a particular material has undergone plastic yielding or not. The Drucker-Prager shear criterion is considered as linear and Drucker-Prager hardening behaviour was defined as compression, having yield stress versus absolute plastic strain. The Drucker-Prager material parameters for the considered soil are given in **Table 7.** The cohesive behavior such as normal stiffness, shear stiffness and tensile strength were taken as 315, 82 and 1 MPa respectively, which is defined as a contact property between tunnel and soil.

3. Finite Element Modelling

The modelling of the concrete, soil, reinforcement as well as acoustic infinite element was carried out using ABAQUS/CAE v.2020. A 0.8 x 0.8 m internal clear square was considered as the size of tunnel, taken exactly similar to the tunnel size as proposed by **Soheyli et al., (2016),** see **Fig 1.** The length, width and height of the model was considered as 12.0, 4.0 and 4.5 m respectively. The thickness of the tunnel lining was considered as 100 mm. A cover of 50 mm was provided on both sides of the tunnel wall. The geometry of soil, concrete and steel reinforcement bars were modelled as solid deformable bodies, **Fig 1(a)-(d).** The tie constraint option available in ABAQUS/CAE was used to provide interaction between concrete and steel, wherein concrete was considered as the host region and the steel was considered as embedded region. The Concrete Damaged Plasticity model and Johnson-Cook model parameters were defined to incorporate the constitutive behaviour of concrete and steel reinforcement. The origin of blast produced by 1.69Kg TNT mass was considered by using

CONWEP model with AIR BLAST definition available in ABAQUS/CAE v.2020. A single layer of main as well as transverse reinforcement were provided with 8mm diameter bars, with 100 mm center to center spacing, see **Fig 1(a) and Fig 1(c).** The strength and failure properties of the steel reinforcement were provided as proposed by **Borvik et al. (2001),** providing a steel section of 460 MPa, however the yield strength of steel reinforcement was 340 MPa, as taken by **Soheyli et al. (2016).** The acoustic infinite element was considered as an acoustic medium with bulk density of 1500 Kg/m^3 and density of 110 Kg/m^3, to define the exterior boundary of the soil strata. ACIN3D4 elements were used in the present study to define the acoustic infinite elements, that are used to define the outer boundary of the model to remove the requirement of impedence type absorbing boundary conditions. A fake contact has been defined between the soil outer surface and the acoustic infinite medium. The connection between the tunnel outer surface and the soil was provided through a surface to surface contact between the two, considering tunnel as the master surface and the surrounding soil as the slave surface. The results thus obtained were compared with that of experimental results as proposed by **Soheyli et al., (2016).**

A detailed mesh convergence study has been conducted, to study the effect of varying mesh size of the tunnel, under consideration on its behaviour towards the blast waves. The mesh size of the tunnel was varied to 50 mm, 40 mm, 30 mm and 20 mm. Total number of elements were 11520, 26800, 63973 and 191400 for the case of 50, 40, 30 and 20 mm mesh size of the concrete tunnel, respectively. The results were recorded in terms of acceleration and von-Mises stresses in the concrete tunnel for varying mesh sizes, as shown in **Fig 2** and **Fig 3.** It has been observed from **Fig 2(a-d).**, that the acceleration value for various mesh sizes is almost same i.e. 2.97 g. The variation of von-Mises stress values for various mesh sizes has been shown in **Fig 3(a-d).** From the mesh convergence study, it can be concluded that 50 mm mesh size is most suitable from computational cost point of view. Hence, 50 mm mesh size can be used for further analysis. The total number of linear hexahedral element of C3D8R were 402888, linear line element type T3D2 were 28080, linear quadrilateral elements of type ACIN3D4 were 1918, quadratic tetrahedral elements of type C3D10M were 5735 and the total number of elements for the standard simulations were 438621.

4. Validation of Finite Element Results

The simulations were carried out against 1.69 Kg TNT mass, placed at a distance of 4m from the surface of the front wall. The constitutive modelling of the steel reinforcement and

the concrete was done by using Johnson-cook model and Concrete Damaged Plasticity model respectively. The Drucker-Prager model has been used to predict the behaviour of the soil, see **section 2**. The use of acoustic infinite elements was employed in order to remove the requirement of impedence- type absorbing boundary conditions on the outer boundary. The finite element modelling of the soil element, along with the RCC tunnel has been explained in **Section 3.** The simulation results, thus obtained were compared with the experimental results as given by **Soheyli et al., (2016). Fig 4** shows the comparison between the actual and the predicted acceleration of the tunnel. The acceleration in the tunnel was noted at the node which was closest to the point of observation, taken in the actual experimental work. The numerical results predicted the pattern of acceleration almost accurately, in the given time step. A good agreement was observed between the acceleration values obtained from the simulation results as well as the experimental results. In general, a maximum deviation of 20% was observed between the actual and the predicted acceleration values of the tunnel. The simulation shows good agreement with the experimental measurements at the final stage, for $t \geq 0.05$ sec. However, at the early stage where $t < 0.05$ sec, it seems that the maximum deviation between the experimental and numerical results is more than 20%, especially in the second and third acceleration peaks. The reason may be due to the fact that the deviation between the parameters of steel reinforcement bars considered in the model and experiment. Moreover, exact parameters for the soil surrounding the tunnel were missing from the literature. Due to the variation between the different parameters used, there is a deviation between the experimental and simulation results. Hence, it was concluded that the present study successfully demonstrates the accuracy of the finite element models of the tunnel.

5. Evaluation of Mitigation Strategies

The simulations were performed on important parameters such as influence of the location of blast, influence of tunnel burial depth, influence of tunnel shapes and influence of varying tunnel lining materials, in order to establish the mitigation strategies of underground tunnels against external surface blast loading. The response of the tunnels was presented in terms of acceleration and von-Mises stresses and the same is discussed in this section.

5.1 Influence of Location of the Blast Source

The simulations were carried out on a 4 m long Square Box shaped tunnel with 0.8x0.8 m clear square cross section and 100 mm thick tunnel lining, subjected to a blast load produced by 1.69 Kg TNT, by placing the blast source at three different locations i.e. externally within

the soil strata at a distance of 4 m horizontally away from the tunnel front wall, internally at the centre of the tunnel (internal blast), and surface blast at a distance of 0.25 m from the top surface of the soil element, for total time period of 0.12 second. The tunnels were buried at a depth of 1 m from the natural ground surface. The acceleration on the inner face of the tunnel front wall against blast load of 1.69 Kg, for three different positions of the blast source, are shown in **Fig 5.** The maximum acceleration was found to be 2337.3 g for the case of internal blast loading, followed by 36.48 g for surface blast loading and 2.97 g for external blast loading. It was also observed that the acceleration reaches its peak within 0.0288 sec from the time of detonation for the case of internal blast loading. However, the peak acceleration was found at 0.0096 and 0.0276 sec for the case of surface blast loading and external blast loading, respectively. The reason for 0.0288 sec from detonation by internal blast loading may be due to the fact that the peak acceleration caused by the reflected waves, whereas the peak acceleration was caused by direct waves at 0.0096 and 0.0276 sec in case of surface blast and external blast loading respectively.

The von-Mises stresses in concrete against blast load of 1.69 kg mass of TNT for different blast positions is shown in **Fig 6.** In case of internal blast loading, the stresses in concrete were found to be 8.09, 10.17 and 9.358 MPa at 0.024, 0.036 and 0.048 Sec respectively. For surface blast loading, the stresses in concrete was 4.24, 4.35 and 4.38 MPa at 0.024, 0.036 and 0.048 Sec respectively. Similarly, for external blast loading, the stresses in concrete were 1.31, 0.20 and 0.14 MPa at 0.024, 0.036 and 0.048 sec respectively. It is observed that the stress in the chosen concrete tunnel was found to be in the range of 10.17-0.14 MPa and however the stress bearing capacity of the concrete is quite high, i.e. 20 MPa. It is concluded that the strength of concrete is more important in case of tunnel against internal blast loading.

The von-Mises stresses in soil element surrounding the tunnel against blast load of 1.69 kg mass of TNT for different blast positions is shown in **Fig 7**. In case of internal blast loading, the stresses in soil element was found to be 0.59, 0.24 and 0.11 MPa at 0.0012, 0.0036 and 0.006 Sec respectively. For surface blast loading, the stresses in soil element were 2.06, 0.44 and 0.27 MPa at 0.0012, 0.0036 and 0.006 Sec respectively. Similarly, for external blast loading, the stresses in soil element were 1.05, 0.55 and 0.25 MPa at 0.0012, 0.0036 and 0.006 sec respectively. It is observed that the sensitivity on soil against surface blast loading is significant. Therefore, it is concluded that the layering of soil filling or depth of the burial of tunnel are more important in case of tunnel against surface blast loading as well as external blast loading.

306 **5.2 Influence of Tunnel Burial Depth**

307 In order to study the influence of burial depth of reinforced concrete tunnel, the
308 simulations on varying tunnel burial depth such as 1, 2 and 3 m were modelled against 1.69 kg
309 mass of TNT placed at a distance of 0.25 m from the top surface of the soil for total time period
310 of 0.12 second, see **Fig 8**. The acceleration on the inner face of the front wall RCC concrete
311 square tunnels at burial depth of 1, 2 and 3 m against surface blast load is shown in **Fig 9**. The
312 maximum acceleration was found to be 36.48, 6.22 and 1.5 g against 1, 2 and 3 m tunnel burial
313 depth respectively. It was observed that the burial depth of the tunnel is significantly reducing
314 the acceleration in the tunnel. It was also clearly seen that the acceleration reaches its peak
315 value within 0.0096 sec from the time of detonation in case of burial depth of 1 m. However,
316 the peak acceleration was observed at 0.0156 and 0.0312 seconds in case of burial depth of 2
317 and 3 m respectively.

318 The von-Mises stresses in the tunnel at varying tunnel burial depth against surface blast
319 load is shown in **Fig 10 a(i)-c(iii).** At 1 m tunnel burial depth, the stresses in concrete were
320 4.24, 4.35 and 4.38 MPa at 0.024, 0.036 and 0.048 Sec respectively. In case of 2 m tunnel
321 burial depth, the stresses in concrete were 2.25, 2.15 and 2.59 MPa at 0.024, 0.036 and 0.048
322 Sec respectively. Similarly, the stresses were found in concrete i.e., 0.72, 0.30 and 0.09 MPa
323 at 0.024, 0.036 and 0.048 Sec respectively at 3 m tunnel burial depth. Overall, it is observed
324 that the stress in concrete was found to be in the range of 4.38 to 0.09 MPa for the chosen mass
325 of TNT. Therefore, it is concluded that the burial depth of the tunnel is one of the important
326 parameter which affects the function of the tunnel against surface blast loading.

327

328 **5.3 Influence of varying tunnel shapes**

329 In order to evaluate the efficiency of the shape of the reinforced concrete tunnel. the
330 square box shape, semi-circular and circular tunnel were modelled against 1.69Kg mass of
331 TNT, placed at a distance of 0.25 m from the top surface of soil for total time period of 0.12
332 second, see **Fig 11**. The acceleration on the inner face of the tunnel front wall of different tunnel
333 shapes is shown in **Fig 12**. The maximum acceleration was found to be 36.48 g for square box
334 shaped tunnel, followed by 16.73g for circular tunnel and 9.56g for semi-circular tunnel. It was
335 also observed that the acceleration reaches its peak within 0.0096 seconds from the time of
336 detonation in case of square box shaped tunnel. However, the peak acceleration was observed
337 at 0.0096 and 0.018 sec in case of semi-circular tunnel and circular tunnel.

338 The von-Mises stresses in reinforced cement concrete of different tunnel shapes against
339 blast load is shown in **Fig 13(a-i)-(c-iii).** In case of square tunnel, the stresses in concrete were

found to be 4.24, 4.35 and 4.38 MPa at 0.024, 0.036 and 0.048 Sec respectively. In semi-circular tunnel, the stresses in concrete were 2.27, 2.42 and 2.67 MPa at 0.024, 0.036 and 0.048 Sec respectively. Similarly, for circular tunnel, the stresses in concrete were 2.20, 2.89 and 3.32 MPa at 0.024, 0.036 and 0.048 Sec respectively. However, it was observed that the stress in the chosen concrete tunnel was found to be in the range of 4.38-2.20 MPa. Among the chosen cases, the circular tunnel offers better performance followed by the semi-circular and square tunnel. The reason for better performance of circular tunnel is may be due to the curvature in nature of tunnel. Therefore, it is concluded that the circular tunnel is one of the best performing tunnel against surface blast loading, among the chosen cases.

5.4 Influence of Tunnel lining materials

The simulations were carried on Reinforced Concrete (RCC), Plain Concrete (PC) and Aluminium lined tunnels against 1.69 Kg mass of TNT, placed at a distance of 0.25 m from the top surface of surrounding soil element of the tunnel, for total time period of 0.12 second. The thickness of RCC, PC and aluminium lining was 100mm. The acceleration on the inner face of the tunnel front wall with different lining materials against blast load is shown in **Fig 14**. The maximum acceleration was found to be 596.1 g for PC, followed by 36.4g for RCC and 16.81g for aluminium. It is also observed that the acceleration reaches its peak value within 0.01092, 0.0096 and 0.0072 seconds from the time of detonation in case of PC, RCC and Aluminium tunnels, respectively. It is concluded that plain concrete is least performing material against blast loading among the chosen cases.

The von-Mises stresses in tunnel having different lining materials against blast load of is shown in **Fig 15 (a-i)-(c-iv)**. In case of PC tunnel, the Mises stresses in tunnel was 3.42, 3.51 and 3.56 MPa at 0.024, 0.036 and 0.048 Sec respectively. In RCC tunnel, the stresses in concrete were 4.24, 4.35 and 4.38 MPa at 0.024, 0.036 and 0.048 Sec respectively. In Aluminium tunnel, the stresses in lining was 1.74, 1.99 and 1.61 MPa at 0.024, 0.036 and 0.048 Sec respectively. However, it was observed that the stress in aluminium tunnel was found to significantly less as compare to PC and RCC. The reason may be due to the fact that the blast resistance capacity of aluminium is significantly higher as compared to other materials.

6. CONCLUSIONS

This paper is focused on the prediction of mitigation strategies of underground tunnels against surface blast loading using finite element technique. The present study has focused to present the best possible measures to safeguard the underground tunnels against the effects of

blast waves. The mitigation of the tunnel damage against surface blast loading has been proposed by providing suitable tunnel lining materials, tunnel burial depth and tunnel shapes. Also, the variation in the tunnel damage intensity through different positions of the blast source, are also discussed in this study.

The simulations were conducted on the underground tunnels against surface blast loading studied considering the different location of blast, influence of tunnel burial depth, influence of tunnel shapes and influence of varying tunnel lining materials. The response of the tunnel was studied in terms of acceleration and Mises stresses and following conclusions were drawn;

- It was observed that the acceleration and von-Mises stress in the tunnel is significantly higher for the case of internal blast loading as compared to the case of external blast loading and surface blast loading. It is concluded that the layering of soil filling or depth of the burial of tunnel are more important in case of tunnel against surface blast loading as well as external blast loading, however, the stress bearing capacity of the concrete is important in case of internal blast loading.
- It is concluded that the burial depth of the tunnel is one of the important parameter which affects the function of the tunnel against surface blast loading. Hence, more is the burial depth of the tunnel, lesser damage would be caused to the tunnel against surface blast loading.
- It is concluded that the circular tunnel is one of the best performing tunnel against surface blast loading, among the chosen cases. Also, it was observed that the square shape tunnel experience the highest acceleration and Mises stress. Hence this shape of the tunnel is most vulnerable against surface blast loading as compared to circular and semi-circular shape tunnel.
- It is concluded that plain concrete is least performing material against blast loading among the chosen cases. The aluminium lined tunnel seems to be the best suitable tunnel lining material among the chosen cases, as the acceleration and von-Mises stress is minimum.

REFERENCES

1. ABAQUS/CAE User's Manual, SIMULIA. Version 6.14.
2. Ambrosini, D., Luccioni, B. (2019). Effects of underground explosions on soil and structures. Underground Space Journal, 5.

3. Ata A, Nabil M, Hassan S, Nawar M. (2021;). Numerical analysis of underground tunnels subjected to surface blast loads. Frat ed Integrita Strutt. 15(55):159–73.
4. Bettelini, M. (2019). Systems Approach to Underground Safety. Underground Space Journal. 5.
5. Borvik, T., Hopperstad, O.S., Berstad, T., Langseth, M. (2001) A computational model of viscoplasticity and ductile damage for impact and penetration. European Journal of Mechanics and Solids 20, 685–712.
6. Dang VK, Dias D, Do NA, Vo TH.(2018) Impact of blasting at tunnel face on an existing adjacent tunnel. International Journal of GEOMATE.15(47):22–31.
7. Gao M, Zhang JY, Chen QS, Gao GY, Yang J, Li DY.(2016) An exact solution for three-dimensional (3D) dynamic response of a cylindrical lined tunnel in saturated soil to an internal blast load. Soil Dynamics and Earthquake Engineering.90:32–7.
8. Goel, M.D., Verma, S. & Panchal, S. (2021) Effect of Internal Blast on Tunnel Lining and Surrounding Soil. Indian Geotechnical Journal 51, 359–368.
9. Hu K, Vafeidis A, Chu C, Zhao Y.(2018) Vibration of a segment tunnel lining under internal blast loading. Journal of Vibroengineering.20(1):448–58.
10. Khan S, Chakraborty T, Matsagar V.(2016) Parametric Sensitivity Analysis and Uncertainty Quantification for Cast Iron–Lined Tunnels Embedded in Soil and Rock under Internal Blast Loading. Journal of Performance of Constructed Facilities. 30(6):04016062.
11. Liu Z, Jiang N, Sun J, Xia Y, Lyu G. (2020;). Influence of tunnel blasting construction on adjacent highway tunnel: A case study in Wuhan, China. International Journal of Protective Structures. 11(3):283–303.
12. Majumder M, Bhattachryya S.(2019) An alternate arrangement of geofoam blocks and air pocket to mitigate confined blast induced vibration. International Journal of Geotechnical Engineering. 00(00):1–14.
13. Mandal J, Agarwal AK, Goel MD.(2020) Numerical Modeling of Shallow Buried Tunnel Subject to Surface Blast Loading. Journal of Performance and Construction Facilities.34(6):04020106.
14. Mandal J, Goel M, Agarwal A. (2021.). Numerical Modeling of Tunnel Subjected to Surface Blast Loading. In: Saha SK, Mukherjee M (eds) Recent Advances in Computational Mechanics and Simulations Lecture Notes in Civil Engineering, vol 103 Springer, Singapore.
15. Mobaraki B, Vaghefi M.(2015) Numerical study of the depth and cross-sectional shape

441 of tunnel under surface explosion. Tunnelling and Underground Space Technology.
442 47:114–22.
443 16. Prasanna R, Boominathan A.(2020) Finite-Element Studies on Factors Influencing the
444 Response of Underground Tunnels Subjected to Internal Explosion. International
445 Journal of Geomechanics. 20(7):04020089.
446 17. Senthil K., Iqbal, M.A., Arindam, B., Mittal, R., Gupta, N.K.. (2018). Ballistic
447 resistance of 2024 aluminium plates against hemispherical, sphere and blunt nose
448 projectiles. Thin-Walled Structures. 126. 94-105.
449 18. Senthil K., Pelecanos L., Rupali S., Prediction of damage intensity of reinforced
450 concrete tunnels and soil against blast loading, 10th International Symposium on
451 Geotechnical Aspects of Underground Construction in Soft Ground, University of
452 Cambridge, 29th June – 01st July 2020, UK (Postponed).
453 19. Senthil K., Sethi M., Pelecanos L., Mitigation Strategies of Underground Tunnels
454 against Blast Loading. International Journal of Protective Structures(Under Review).
455 20. Soheyli, M.R., Akhaveissy, A.H., Mirhosseini, S.M. (2016) Large-scale experimental
456 and numerical study of blast acceleration created by close-in buried explosion on
457 underground tunnel lining. Shock and Vibration. 2016, Article ID 8918050.
458 21. Tiwari R, Chakraborty T, Matsagar V.(2016) Dynamic Analysis of Tunnel in
459 Weathered Rock Subjected to Internal Blast Loading. Rock Mechanics and Rock
460 Engineering. 49(11):4441–58.
461 22. Vinod, M.,Khabbaz, H. (2019). Comparison Of Rectangular And Circular Bored Twin
462 Tunnels In Weak Ground. Underground Space Journal, 4.
463 23. Xia X, Li HB, Li JC, Liu B, Yu C.(2013) A case study on rock damage prediction and
464 control method for underground tunnels subjected to adjacent excavation blasting.
465 Tunnelling and Underground Space Technology.35:1–7.
466 24. Yang Y, Xie X, Wang R.(2010) Numerical simulation of dynamic response of
467 operating metro tunnel induced by ground explosion. Journal of Rock Mechanics and
468 Geotechnical Engineering.2(4):373–84.
469 25. Yu H, Wang Z, Yuan Y, Li W.(2015) Numerical analysis of internal blast effects on
470 underground tunnel in soils. Structure and Infrastructure Engineering. 12(9):1090–105.
471 26. Zhang GY, Xie W, Yang QG, Luo J. (2021) Research on open cut blasting technology
472 of reservoir diversion tunnel. International Journal of Critical Infrastructures.
473 2021;17(1):21-37.
474 27. Zhao PJ, Lok TS, Yin ZQ, Zhou ZL.(2010) Simplified design of rock cavern concrete

lining to resist shock loading. Journal of Central South University of Technology.17:1087-1094.

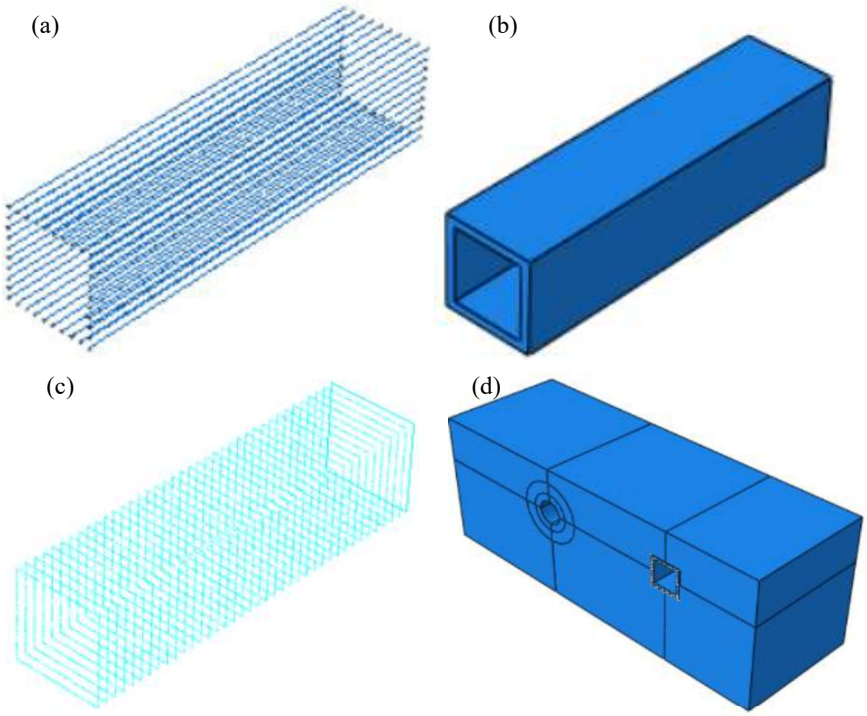

Fig 1. Tunnel (a) longitudinal reinforcement bar (b) concrete (c)transverse reinforcement bar (d) isometric view of combined finite element model

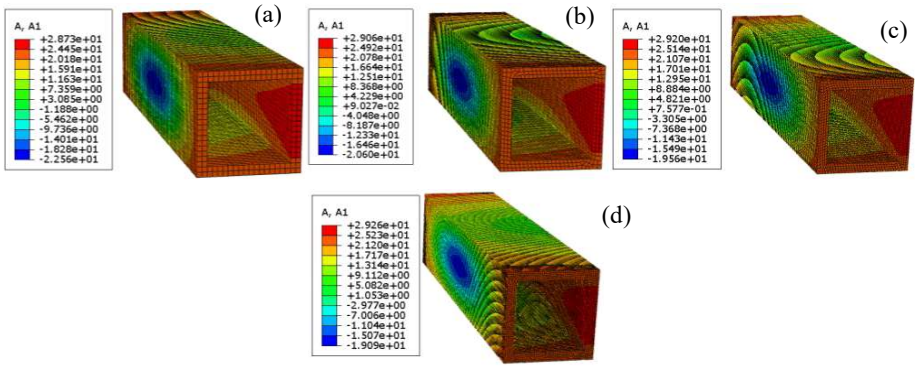

Fig 2. Acceleration in concrete tunnel at (a) 50mm (b) 40mm (c) 30mm and (d) 20 mm mesh size

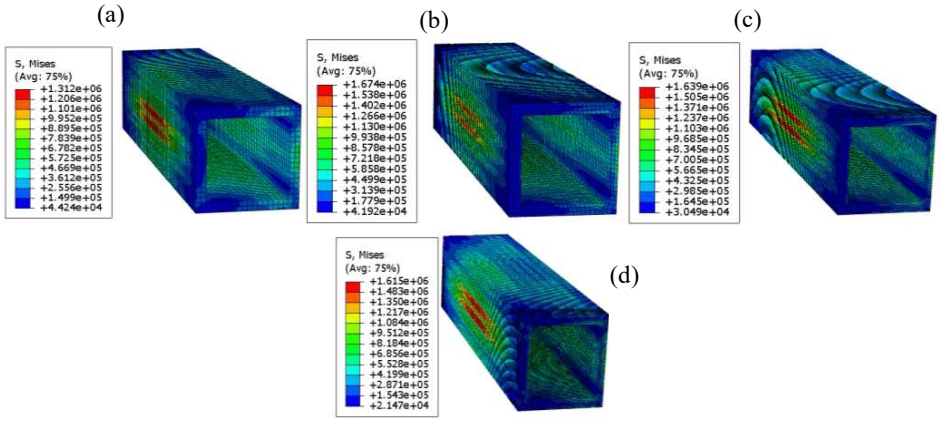

Fig 3. Mises stresses in concrete tunnel at (a) 50mm (b) 40mm (c) 30mm and (d) 20 mm mesh size

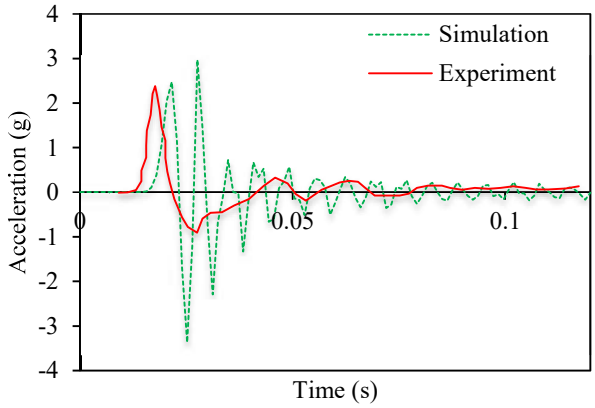

Fig 4. Comparison of acceleration obtained from simulation and experiment with 1.69 Kg mass of TNT at a distance of 4 m from the tunnel front wall

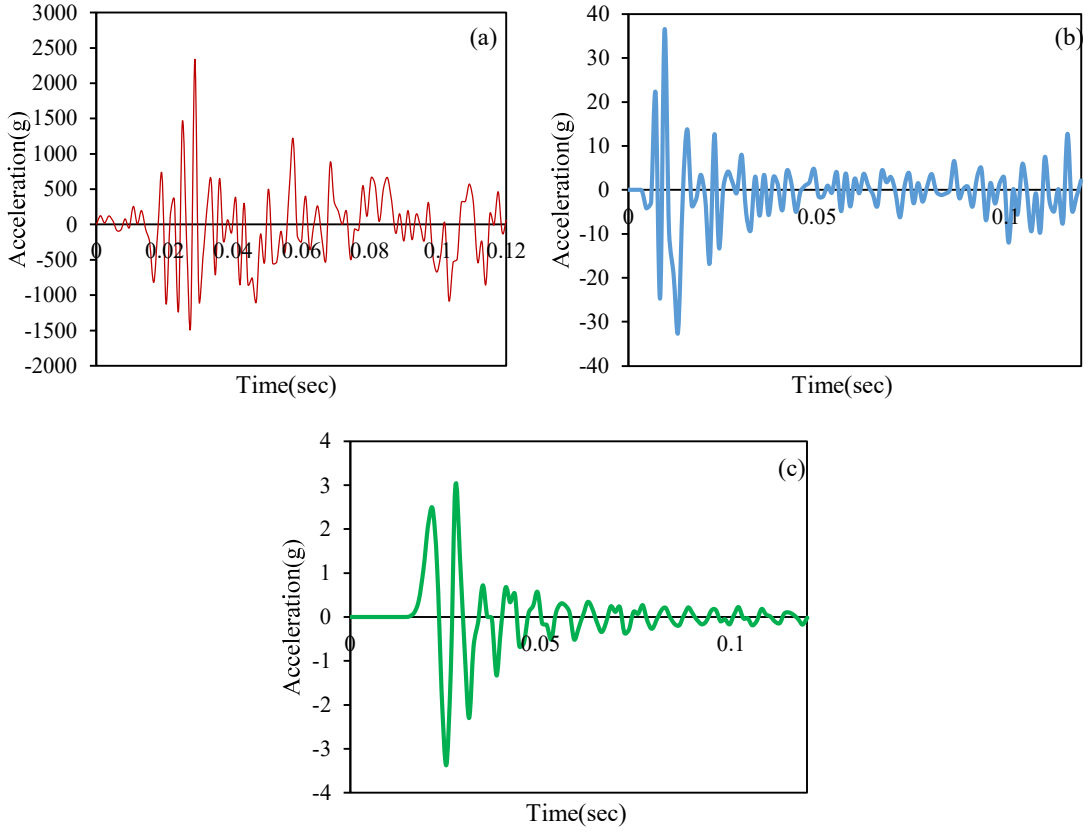

Fig 5. Acceleration function of time in the tunnel against (a) internal blast (b) surface blast and (c) external blast loading

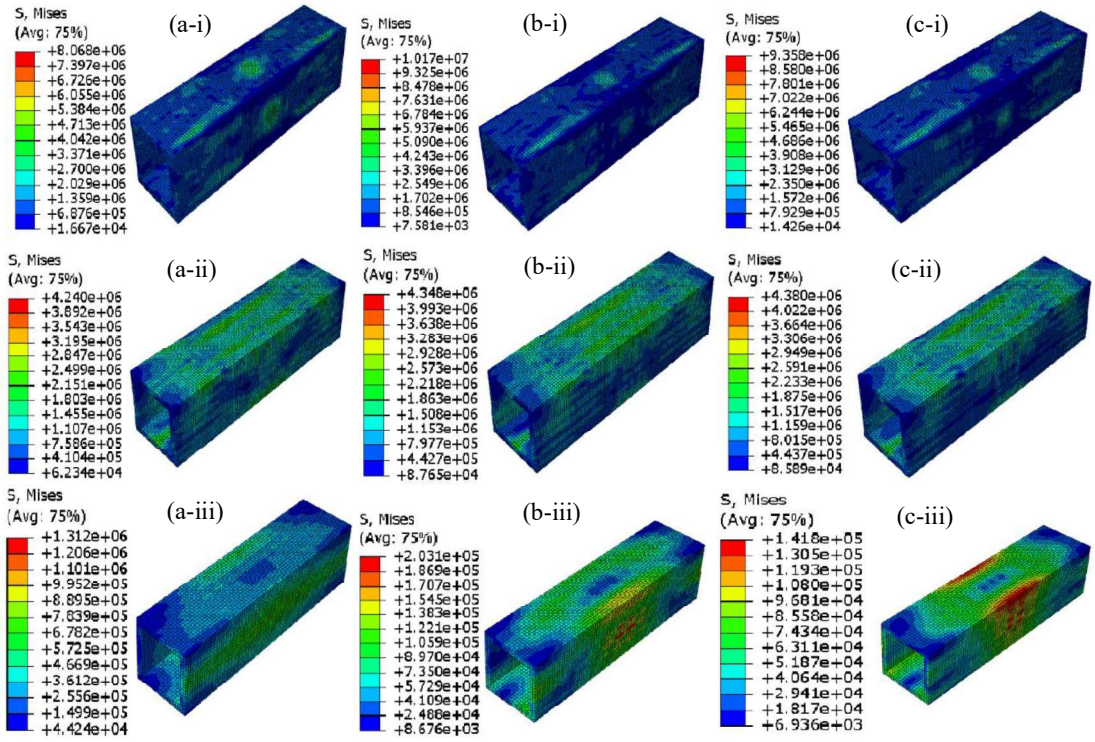

Fig 6. Mises stress in the tunnel front wall at (a) 0.024 (b) 0.036 and (c) 0.048 sec against (i) internal (ii) surface and (iii) external blast loading

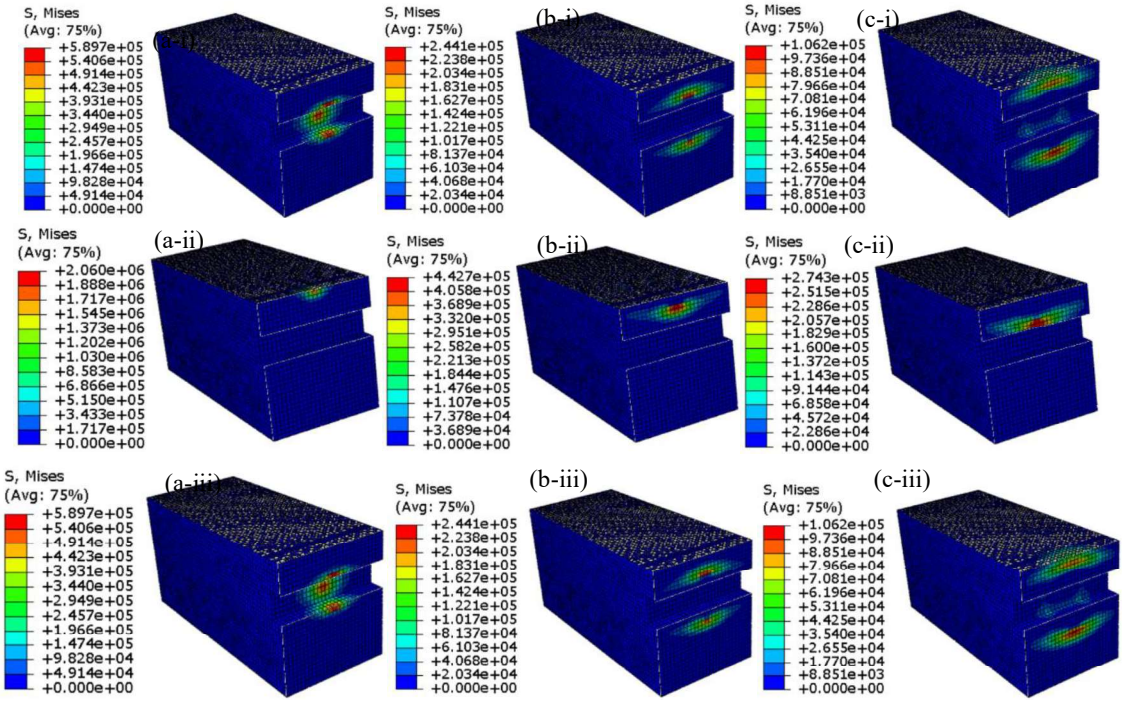

Fig 7. Mises stress in the tunnel front wall at (a) 0.0012 (b) 0.0036 and (c) 0.006 sec for (i) internal (ii) surface and (iii) external blast loading

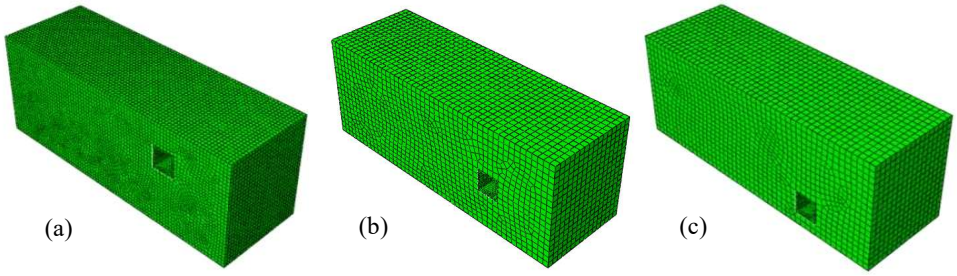

Fig 8. Tunnel at (a) 1 (b) 2 and (c) 3 m burial depth

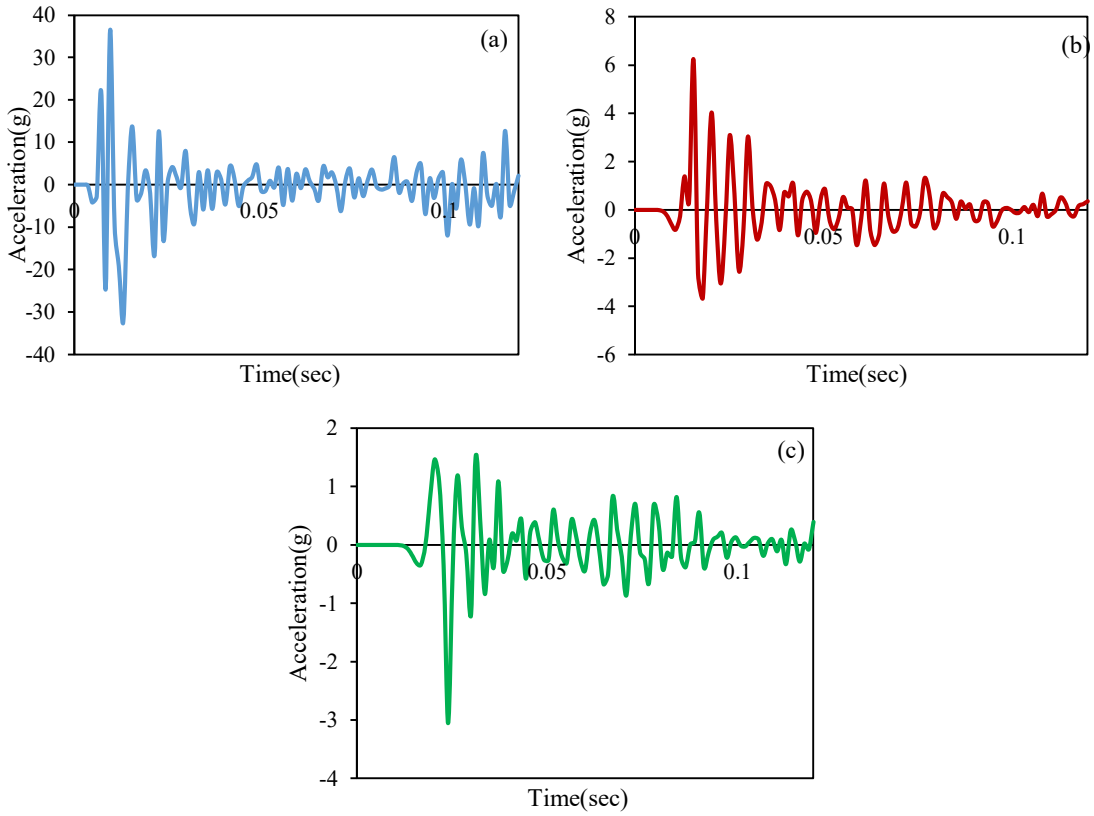

Fig 9. Acceleration in tunnel having burial depth (a) 1 (b) 2 and (c) 3 m against surface blast loading

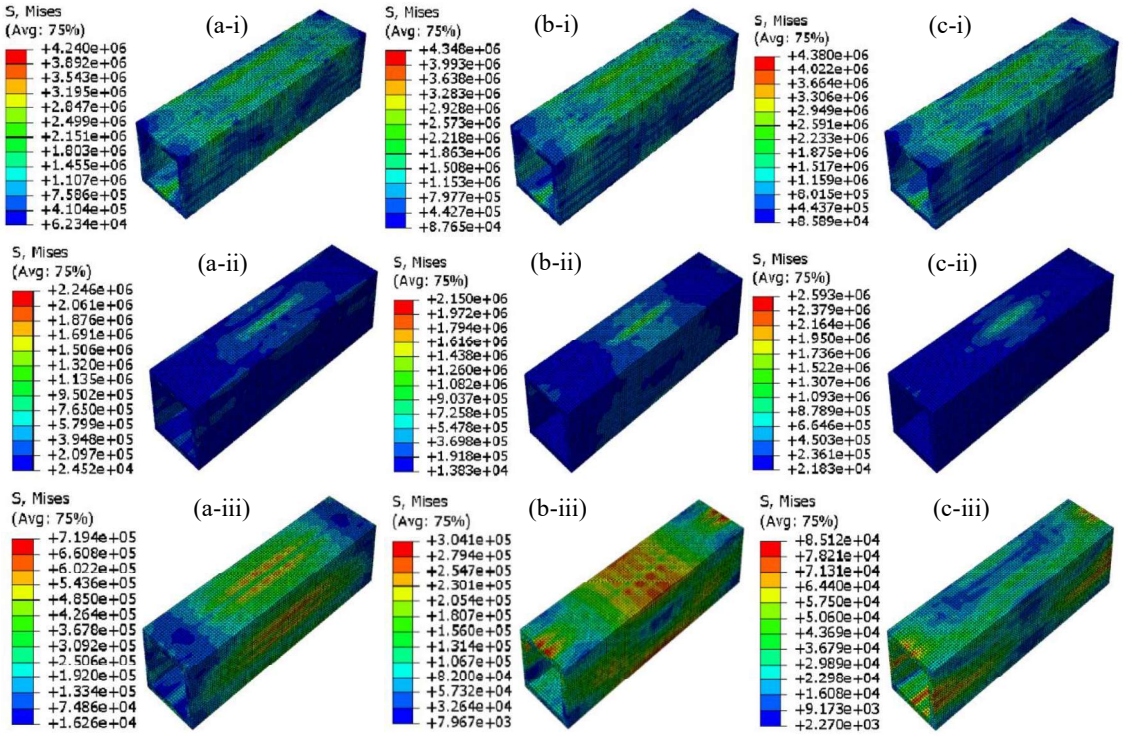

Fig 10. Mises stress in the tunnel front wall at (a) 0.024 (b) 0.036 and (c) 0.048 sec for surface blast loading at (i) 1 (ii) 2 and (iii) 3 m burial depth

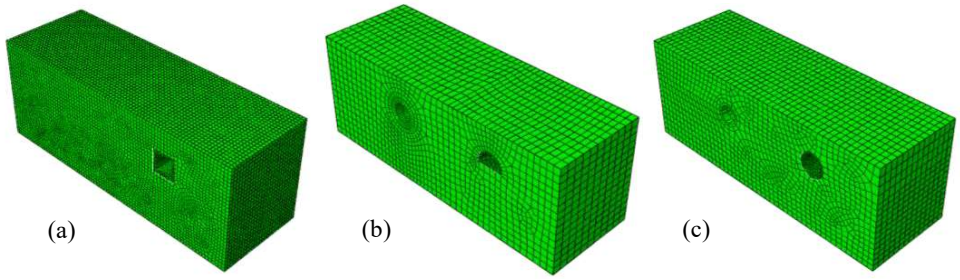

Fig 11. Tunnel with (a) square (b) semicircular and (c) circular shapes

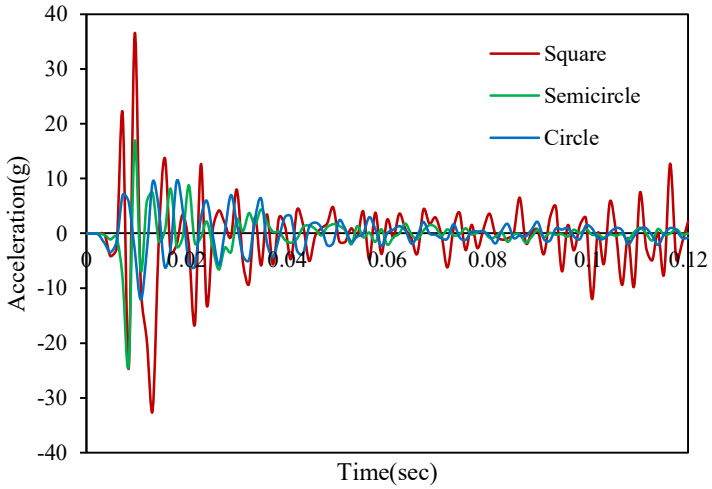

Fig 12. Acceleration in tunnel having different tunnel shapes against surface blast loading

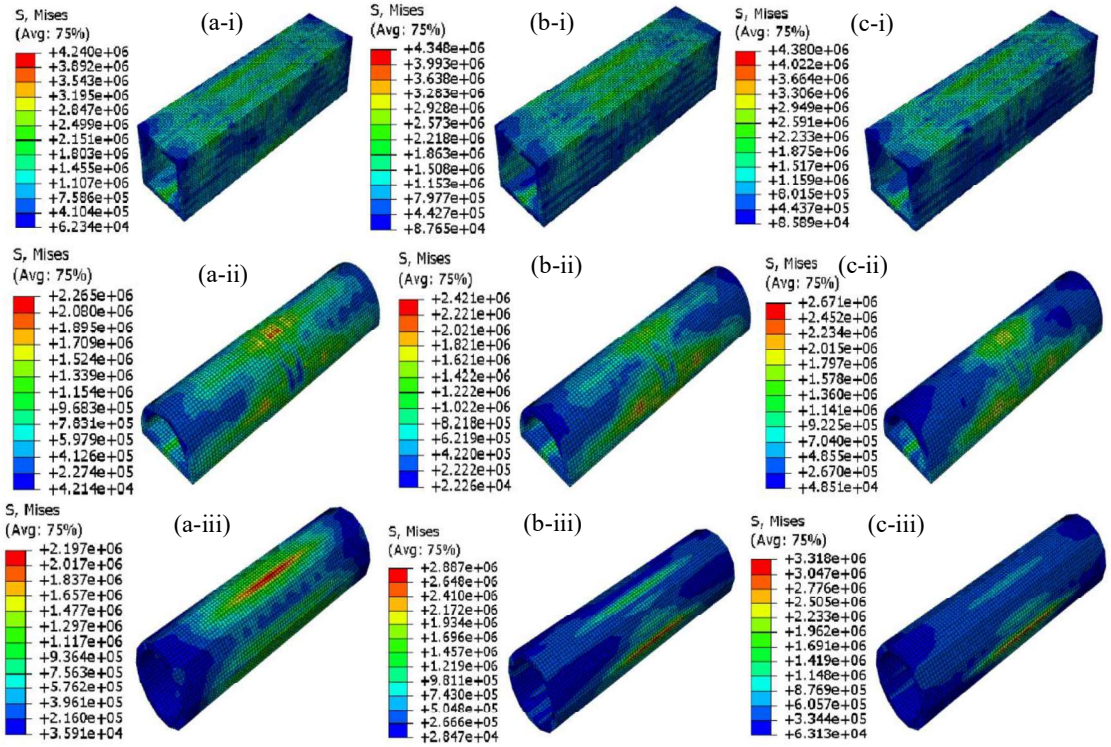

Fig 13. Mises stress in (i) square (ii) semicircular and (iii) circular tunnel against surface blast loading at (a) 0.024 (b) 0.036 and (c) 0.048 sec

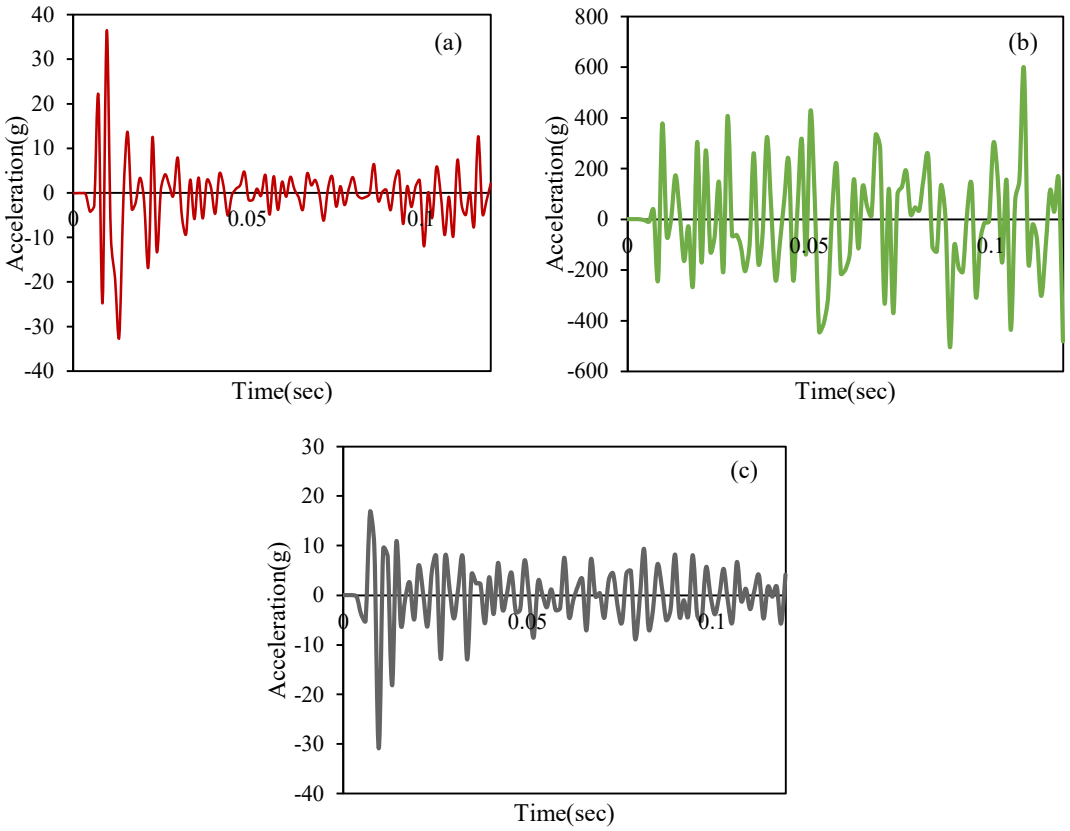

Fig 14. Acceleration in (a) reinforced cement concrete (b) plain cement concrete and (c) aluminum lining tunnels against surface blast loading

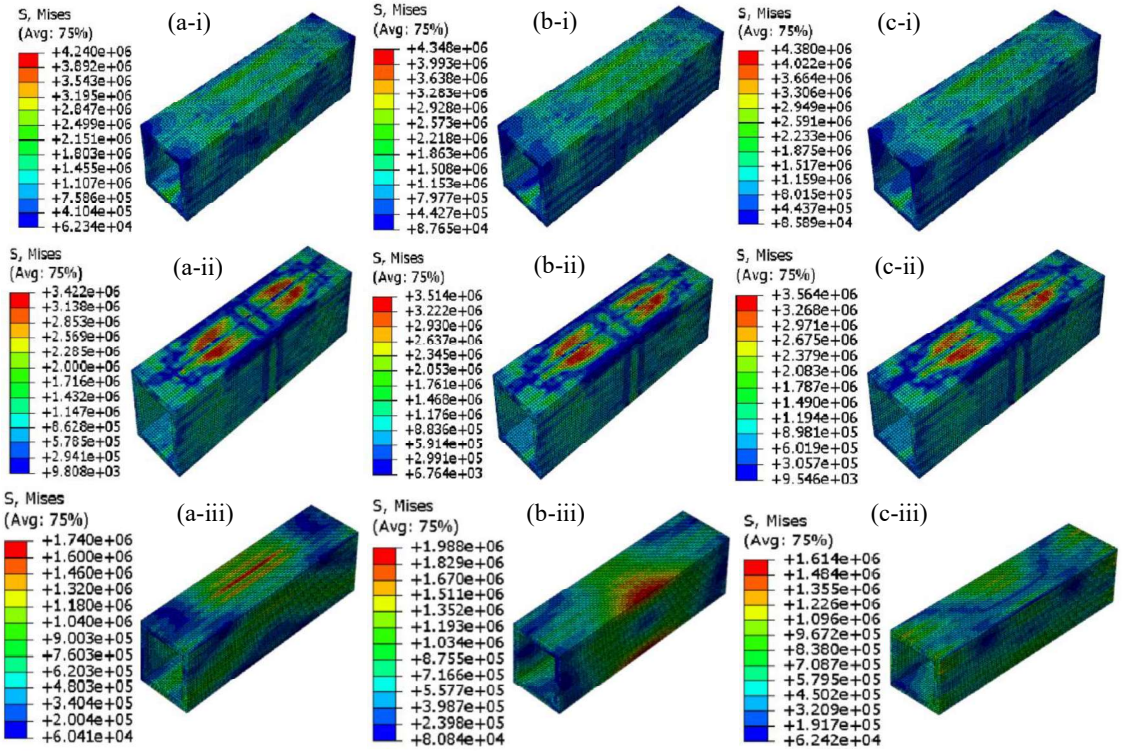

Fig 15. Mises stress in (i) RCC (ii) PC and (iii) Aluminum lining tunnels against surface blast loading at (a) 0.024 (b) 0.036 and (c) 0.048 sec

Table 1 Material constant for Aluminium and Steel

Description		Aluminium 2024 [Senthil et al. (2018)]	Weldox 460E [Borvik et al (2001)]
Density (kg/m^3)		2710	7850
Young's Modulus (N/mm^2)		71000	200000
Poisson's ratio		0.33	0.33
Yield stress constant A (N/mm^2)		265	490
Strain hardening constant B (N/mm^2)		426	807
n		0.34	0.73
Viscous effect C		0.015	0.0114
Thermal softening constant m		1	0.94
Reference strain rate $\varepsilon_\circ$		1	0.0005
Melting temperature (K)		893	1800
Transition temperature (K)		293	293
Fracture strain Constant	D_1	0.13	0.0705
	D_2	0.13	1.732
	D_3	-1.5	-0.54
	D_4	0.011	-0.015
	D_5	0	0

Table 2 Material constants for concrete material [Senthil et al. (2020)]

Description	Numerical Value
Density (kg/m^3)	2400
Young's Modulus (N/mm^2)	19700
Poisson's ratio	0.2
Dilation angle	35°
Eccentricity(m)	0.1
K	0.66
$\sigma_{b0/\sigma c0}$	1.16

Table 3 Concrete compressive behavior [Senthil et al. (2020)]

Yield stress (N/mm^2)	Inelastic strain
20.0	0
19.8	0.00015
19.6	0.00025
19.4	0.00035
19.1	0.00045
18.8	0.00055
18.5	0.00065
18.1	0.00075
17.7	0.00085
17.4	0.00095
17.0	0.00105
16.6	0.00115
16.3	0.00125
15.9	0.00135
15.5	0.00145
15.2	0.00155
14.9	0.00165
14.5	0.00175
14.2	0.00185
13.9	0.00195
13.6	0.00205
13.3	0.00215
13.0	0.00225

Table 4 Concrete tensile behavior [Senthil et al. (2020)]

Yield stress (N/m^2)	Cracking strain
1.80	0
1.50	0.00012
0.60	0.00024
0.10	0.00065
0.05	0.00080

Table 5 Concrete compression damage [Senthil et al. (2020)]

Damage parameter d_c	Inelastic strain
0	0
0.006	0.00015
0.015	0.00025
0.027	0.00035
0.041	0.00045
0.057	0.00055
0.074	0.00065
0.092	0.00075
0.110	0.00085
0.129	0.00095
0.148	0.00105
0.166	0.00115
0.18	0.0012
0.20	0.0013
0.22	0.0014
0.23	0.0015
0.25	0.0016
0.27	0.0017
0.28	0.0018
0.30	0.0019
0.31	0.0020
0.33	0.0021
0.34	0.0022

Table 6 Concrete tensile damage [Senthil et al. (2020)]

Damage Parameter	Cracking Strain
0	0
0.40	0.00012
0.69	0.00024
0.92	0.00065

Table 7 Material constant for soil [Senthil et al. (2020)]

Density (kg/m^3)	Elastic modulus (N/mm^2)	Poisson ratio	Dilatation angle	Friction angle	Flow stress ratio
1850	29	0.36	1	31	0.778